Foot and Ankle Surgery 25 (2019) 771–781

Contents lists available at ScienceDirect

Foot and Ankle Surgery

journal homepage: www.elsevier.com/locate/fas

Reliability of distal tibio-fibular syndesmotic instability measurements using weightbearing and non-weightbearing cone-beam CT

Greg M. Osgood[a], Delaram Shakoor[b,*], Jakrapong Orapin[c,d], Jianzhong Qin[c,e], Iman Khodarahmi[b], Gaurav K. Thawait[b], James R. Ficke[a], Lew C. Schon[c], Shadpour Demehri[b]

[a] Department of orthopedic surgery, The Johns Hopkins University School of Medicine, Baltimore, MD, USA
[b] Department of Radiology and Radiological Science, The Johns Hopkins University School of Medicine, Baltimore, MD, USA
[c] Department of Foot and Ankle Surgery, MedStar Union Memorial Hospital, Baltimore, MD, USA
[d] Department of Orthopedic Surgery, Ramathibodi Hospital, Mahidol University, Bangkok, Thailand
[e] Department of Orthopedic Surgery, The Second Affiliated Hospital of Soochow University, Suzhou, China

A R T I C L E I N F O

Article history:
Received 21 February 2018
Received in revised form 22 July 2018
Accepted 14 October 2018

Keywords:
Syndesmotic injury
Weightbearing
Cone-beam computed tomography
Non-weightbearing

A B S T R A C T

Background: To investigate the reliability and reproducibility of syndesmosis measurements on weightbearing (WB) cone-beam computed tomography (CBCT) images and compare them with measurements obtained using non-weightbearing (NWB) images.
Methods: In this IRB-approved, retrospective study of 5 men and 9 women with prior ankle injuries, simultaneous WB and NWB CBCT scans were taken. A set of 21 syndesmosis measurements using WB and NWB images were performed by 3 independent observers. Pearson/Spearman correlation and intra-class correlation (ICC) were used to assess intra- and inter-observer reliability, respectively.
Results: We observed substantial to perfect intra-observer reliability (ICC = 0.72–0.99) in 20 measurements. Moderate to perfect agreement (ICC = 0.45–0.97) between observers was noted in 19 measurements.
Conclusion: Measurements evaluating the distance between tibia and fibula in the axial plane 10 mm above the plafond had high intra- and inter-observer reliability. Mean posterior tibio-fibular distance, diastasis, and angular measurement were significantly different between WB and NWB images.

1. Introduction

The distal tibio-fibular syndesmosis provides dynamic stability to the ankle joint and maintains the integrity of ankle mortise during weightbearing [1,2]. Syndesmotic injuries occur commonly after ankle trauma and are associated with 10% of all ankle sprains and 11%–50% of ankle fractures [2,3]. Biomechanical studies have shown that minor alterations in mortise congruity as a result of an unstable syndesmosis can significantly increase tibio-talar articular surface contact pressure [4]. Therefore, early detection of syndesmotic injury, along with restoration of its anatomic relation, are critical to preventing devastating long-term outcomes, including secondary tibio-talar osteoarthritis [5].

Early and accurate detection of syndesmotic injuries is a critical but challenging task, which has been addressed by several radiographic measurements. However, these measurements have provided highly variable and unreliable results because of wide anatomic variation in the shape of the tibial tubercles and depth of the fibular groove, as well as the effect of ankle positioning during plain radiographic studies [3,4,6–9]. Therefore, advanced imaging modalities, such as computed tomography (CT) and magnetic resonance imaging (MRI), are being used increasingly for radiographic assessment of syndesmotic injuries [4,10,11].

Several CT-based measurements have been proposed to describe cross-sectional anatomy of the syndesmosis. Although studies have reported high reliability and reproducibility of these CT measurements, most of these studies have been performed on

Abbreviations: ATFD, anterior tibio-fibular distance; CBCT, cone-beam computed tomography; CT, computed tomography; ICC, intra-class correlation coefficient; LCS, lateral clear space; MCS, medial clear space; MRI, magnetic resonance imaging; NWB, non-weightbearing; PTFD, posterior tibio-fibular distance; TFCS, tibio-fibular clear space; LI, tibial incisura length line; WB, weightbearing.

* Corresponding author at: Department of Radiology and Radiological Science, The Johns Hopkins University School of Medicine, 601 North Caroline Street, Baltimore, MD, USA.
E-mail addresses: dshakoo1@jhmi.edu, delaramshakoor@mail.com (D. Shakoor)
.

https://doi.org/10.1016/j.fas.2018.10.003
1268-7731/

cadavers or asymptomatic patients [4,8–10,12–17]. Furthermore, studies have shown that the use of weightbearing (WB) CT is associated with higher diagnostic accuracy in the assessment of other foot and ankle biomechanical derangements [18–23], and there is no evidence regarding reliability of these measurements obtained from WB images.

In this exploratory study, we tested the reliability and reproducibility of syndesmosis measurements in patients with prior ankle injuries using WB cone-beam computed tomography (CBCT) images and compared these measurements with those obtained from non-weightbearing (NWB) images.

2. Material and methods

This retrospective (level 3) study complies with the Declaration of Helsinki and the Health Insurance Portability and Accountability Act. Our institutional review board approved the study, and all study participants provided written informed consent.

2.1. Study design and participants

Between October 2014 and July 2017, 20 patients with a history of ankle injury (supination or pronation external rotation injury) underwent WB CBCT in our department. All patients had completed treatment before the examination, and WB CBCT scans were performed when the referring physician allowed the patient to fully bear weight. The mean (± standard deviation) interval between injury and the CBCT examination was 78 ± 59 days. The decision between operative and non-operative treatment was made by 2 board-certified orthopedic surgeons on the basis of the stability criteria at the patient's first clinical visit [24,25]. Among these 20 patients, 6 fractures were unstable and received operative treatment, and 14 fractures were treated non-operatively. The patients were referred to us for further evaluation because functional outcomes at their last follow-up visits were unsatisfactory (i.e., pain, activity limitation). We included fractures that were stable at the first clinic visit and thus received non-operative treatment. The participants consisted of 5 men and 9 women with mean age of 50 (range 27–75) years and mean BMI of 31.8 (range 19.5, 53.5). Ten right ankles and 4 left ankles were scanned. Patients had 7 Weber B fractures, 2 Weber C fractures, and 5 isolated ankle sprains without simultaneous fracture. In all examinations, the injured ankle was scanned under both WB and NWB conditions.

2.2. CBCT imaging technique

All CT examinations were obtained on a CBCT extremity scanner (generation II, Carestream Health, Inc., Rochester, NY). Two consecutive scans of the symptomatic ankle were performed: 1 NWB scan in which participants sat on a chair with the knee and ankle in extended and neutral positions, respectively, while the foot was placed plantigrade on a foam surface in the CBCT gantry, and 1 WB scan. For the WB position, the patient was standing with

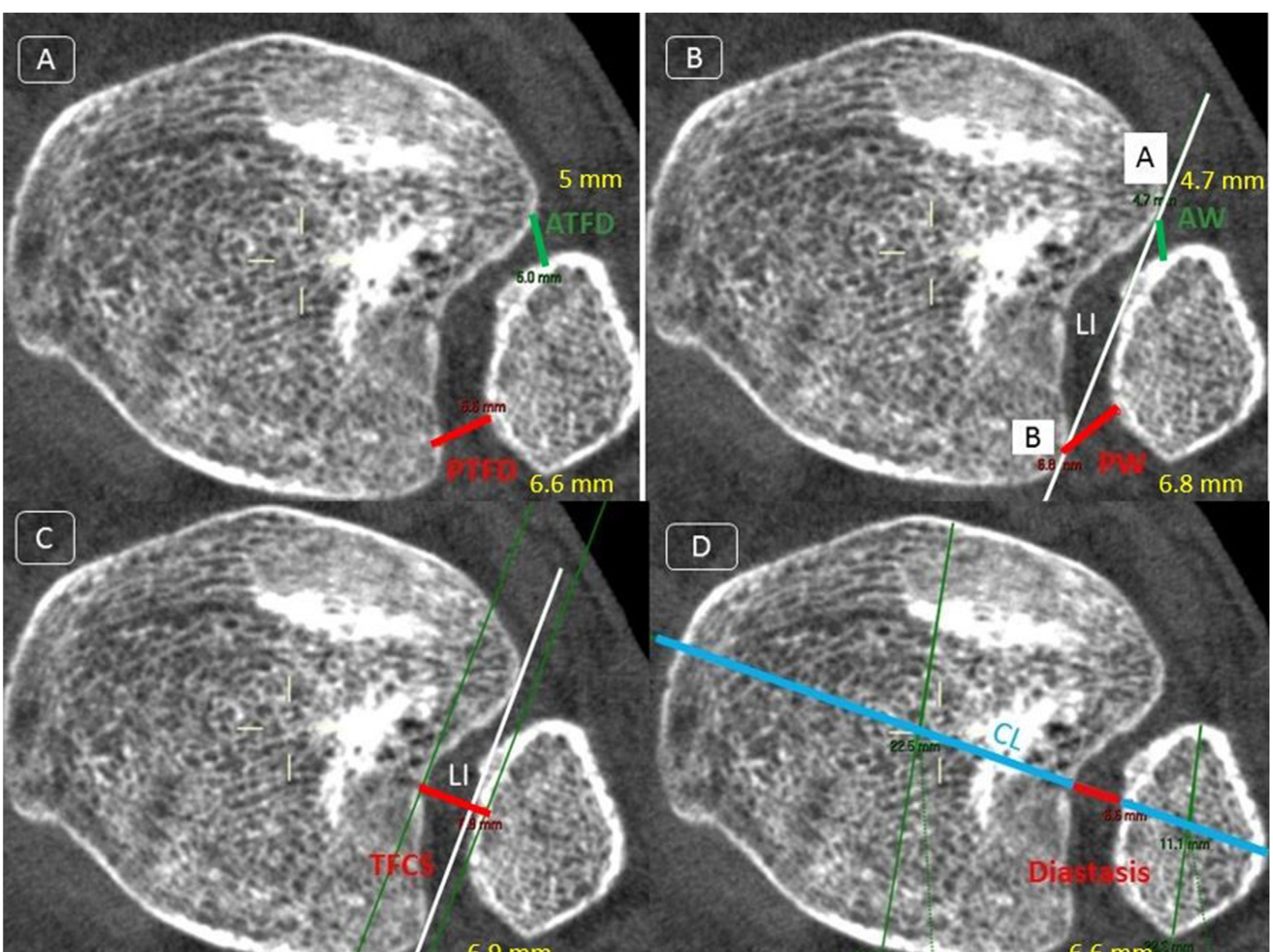

Fig. 1. Depiction of diastasis measurements. Axial images were set at 10 mm above the tibial plafond. (A) ATFD: anterior tibio-fibular distance, PTFD: posterior tibio-fibular distance. (B) LI: tibial incisura length line, AW: anterior width, PW: posterior width. (C) TFCS: tibio-fibular clear space. (D) Diastasis, CL: central line.

feet at approximately shoulder width and body weight distributed evenly between legs. We used the same scan protocol used in prior technical assessments [26]. We applied 72 mAs and 90 kVp for all scans to enhance contrast-to-noise ratio per unit of dose within the boundaries of our CT system power. The conversion factor for size-specific dose estimates was 1.4 for the foot and ankle (8 cm); thus, the size-specific dose estimate for CBCT ankle imaging was calculated to be 12 mGy.

We used a Farmer chamber in a stack of three 16-cm CT dose index phantoms and observed that the weighted CT dose index was approximately 15 mGy [27]. To reconstruct images with 0.5-mm^3 isotropic voxels, we applied a "bone" algorithm using iterative reconstruction.

2.3. Measurements

The raw 3D data were used to generate axial, coronal, and sagittal image slices, which were transferred into exclusive software (Vue PACS, Carestream Health, Inc.) to obtain computer-based measurements. Image annotations were removed during analysis, and each study was assigned a random, unique number. Each observer underwent a training program with 5 asymptomatic cases that were not included in the current study and learned how to obtain the measurements using the software. One musculoskeletal fellowship–trained radiologist (observer 1), 1 fellowship-trained foot and ankle surgeon with 10 years of clinical experience (observer 2), and 1 fellowship-trained foot and ankle surgeon with 5 years of clinical experience (observer 3) obtained the measurements in a random, blinded, independent approach. One month after the first assessment (washout period), a second set of measurements was obtained by the foot and ankle surgeon to evaluate intra-observer reliability.

After a thorough literature search, we performed 4 distinct categories of measurements based on the concept being evaluated: (1) diastasis-related measurements; (2) rotation measurements; (3) translation measurements; and (4) malleolar and talar measurements.

2.4. Diastasis

We performed 7 diastasis measurements in the axial plane. The axial plane was defined as exactly parallel to the tibial plafond and was set at 10 mm above the tibial subchondral bone.

Measurements 1 and 2: anterior and posterior tibio-fibular distances. As described by Elgafy et al. [12], the first measurement was anterior tibio-fibular distance (ATFD), which was the closest distance between the anterior tibial tubercle and the anterior border of fibula (Fig. 1A). The second measurement was posterior tibio-fibular distance (PTFD), which was the shortest distance between the medial border of the fibula and posterior tibial tubercle (Fig. 1A).

Measurements 3 and 4: anterior and posterior widths. We performed 2 measurements described by Lepojärvi et al. [28]. To obtain these 2 measurements, the tibial incisura length line (LI) was established by drawing a line tangential to the most prominent parts of the anterior and posterior tibial tubercles. We used the intersections of this line with the tibial tubercles as our reference points A and B. To determine the anterior and posterior widths, we measured the shortest distances between A and B with the medial border of fibula, respectively (Fig. 1B).

Measurement 5: tibio-fibular clear space (TFCS). We performed TFCS measurements as described by Lepojärvi et al. [17]. We drew 2 tangential lines to the deepest points of fibularis incisura and medial border of fibula, parallel to the LI. Then we measured the distance between these 2 tangential lines (Fig. 1C).

Measurement 6: diastasis. As described by Prior et al. [13], we first determined the center of the tibia and fibula by measuring the distance between the anterior and posterior borders of each bone and determined the center of those lines. We then drew the center line that connected the center points of the tibia and fibula. Diastasis was measured as the distance between the medial cortex of the fibula and the lateral cortex of the tibia along the center line (Fig. 1D).

Measurement 7: angular measurement. We performed angular measurement as described by Malhotra et al. [29]. We calculated the angle between the lines that were tangential to the anterior and posterior parts of tibia and lateral malleolus (Fig. 2).

2.5. Rotation of the fibula

We performed 4 rotation measurements in the same axial plane as described earlier.

Measurement 8: rotation of fibula (1): The first measurement, described by Lepojärvi et al. [17], was the angle between the LI and tangent of the anterolateral cortex of the fibula (Fig. 3A).

Measurement 9: rotation of fibula (2): The second measurement, described by Dikos et al. [9], was the angle between the LI and the line across the anterior and posterior fibular tubercles (Fig. 3B).

Measurement 10: rotation of fibula (3): The third measurement, described by Zwipp et al. [30] and Vasarheyi et al [31], was the angle between the tangential line to the most anterior point of the anterior surface of the tibia and the bisection of the vertical axis of the fibula (Fig. 3C). The normal absolute value of this measurement is reported to be approximately 90°. We used the approach of Knops et al [32] and subtracted 90° from the absolute values.

Measurement 11: rotation of fibula (4): The fourth measurement, described by Tang et al. [33], was the ratio of 2 distances. First, we drew multiple, bisecting lines over the tibia and determined the summation of the intersections as the center reference point. We then measured the distances from this reference point to the most anterior and posterior cortices of the fibula (Fig. 3D). The ratio was calculated by dividing the anterior distance by the posterior distance.

2.6. Translation of the fibula

We performed 4 translation measurements in the same axial plane, as described earlier.

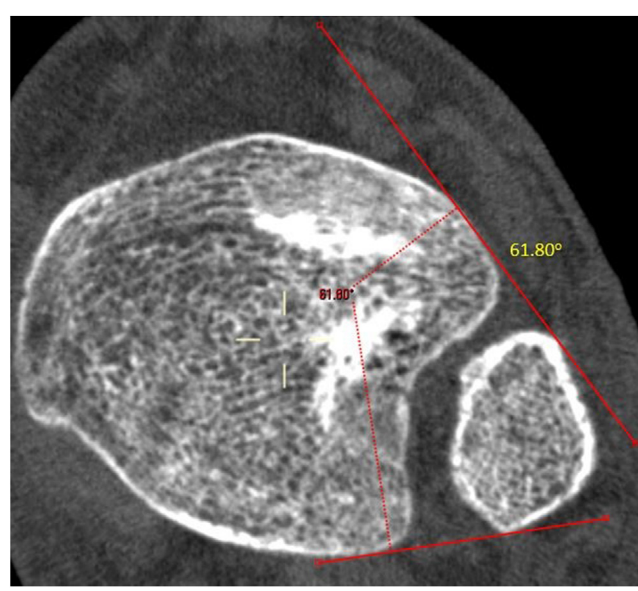

Fig. 2. Depiction of angular measurement. Axial images were set at 10 mm above the tibial plafond.

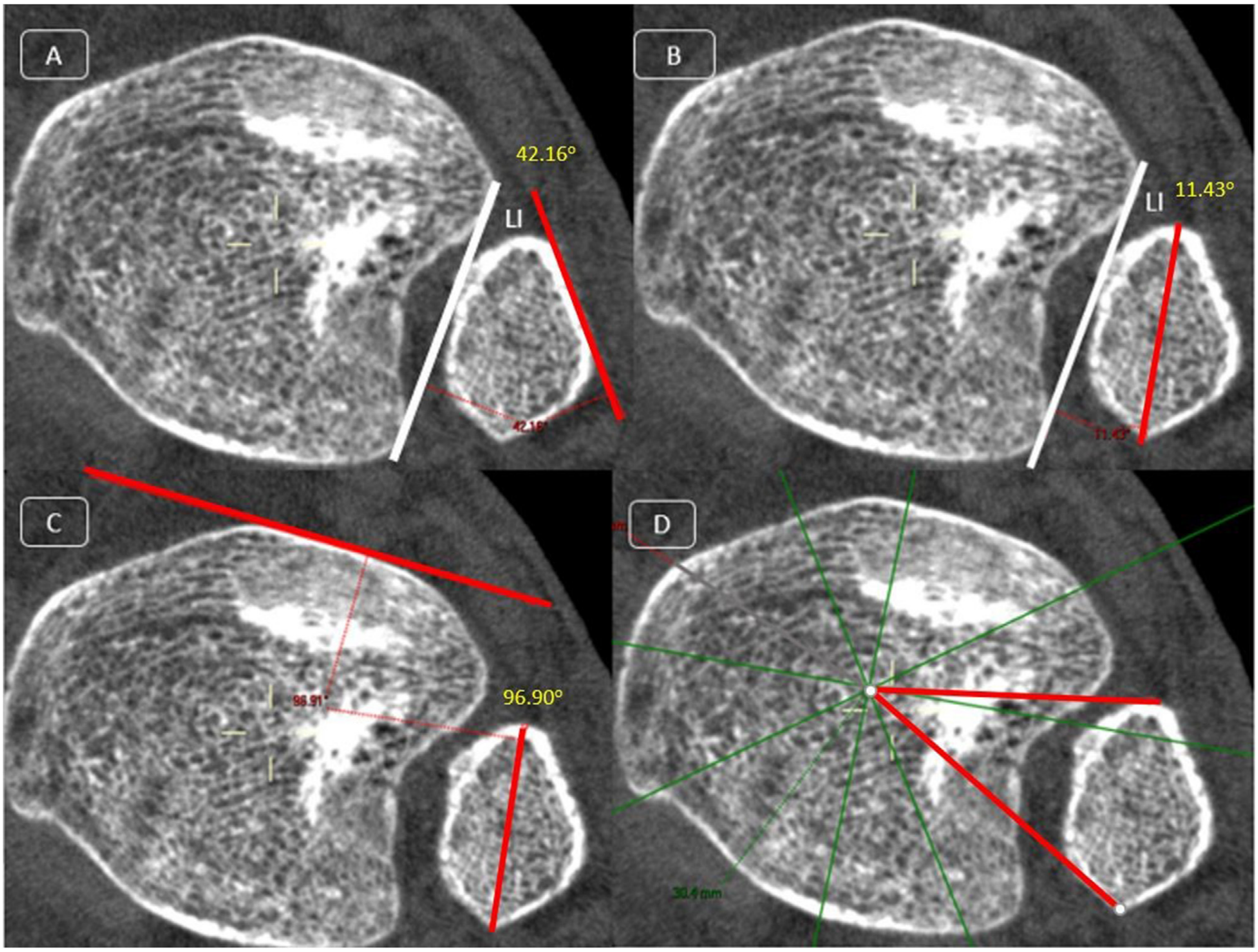

Fig. 3. Depiction of rotation measurements. Axial images were set at 10 mm above the tibial plafond. (A) Rotation of fibula 1. (B) Rotation of fibula 2 (LI: tibial incisura length line). (C) Rotation of fibula 3. (D) Rotation of fibula 4.

Measurement 12*: translation measurement (*1*)*: The first measurement was described by Phisitkul et al. [34]. Reference line A was drawn as a perpendicular line to the LI at the anterior tibial tubercle. We then measured the distance from the most anterior point of the fibula to reference line A. If the fibula was posterior to reference line A, the value was positive, and if it was anterior to reference line A, it was negative (Fig. 4A).

Measurement 13: *translation measurement (*2*)*: The second measurement was described by Lepojärvi et al. [28]. First, we drew a line parallel to the LI between the anterior and posterior margins of the fibula. We then measured the distance between the midpoints of the parallel line and the LI (Fig. 4B).

Measurement 14: *translation measurement (*3*)*: The third measurement was described by Prior et al [13]. First, we established reference line B by drawing a parallel line to the center line and placed it on the most anterior part of the tibia. The translation measurement was the distance from the most anterior part of fibula to reference line B, drawn parallel to the LI (Fig. 4C).

Measurement 15*: translation measurement (*4*)*: The fourth measurement was described by Davidovitch et al. [14]. First, we drew a line connecting the most anterior and posterior points of the fibula. Then, from the most anterior point we drew a perpendicular line and established it as reference line C. We then drew a parallel line to reference line C at the anterior tibial tubercle. The distance between reference line C and the parallel line was the fourth translation measurement (Fig. 4D).

2.7. Other measurements

Measurement 16*: bimalleolar angle.* We measured the bimalleolar angle as described by Nault et al [10]. We set the axial plane at the level of and exactly parallel to the talar dome. We then measured the angle between the talar sides of the 2 malleoli (Fig. 5A).

Measurements 17 *and* 18*: medial and lateral clear spaces.* These measurements were made at the axial plane exactly parallel to and 5 mm below the talar dome. The medial clear space (MCS) and lateral clear space (LCS) were measured as the distances between the talus and the medial and lateral malleoli, respectively [35,36] (Fig. 5B).

Measurement 19*: talar rotation.* To measure talar rotation, we set the axial plane exactly parallel to the tibial plafond, 1 mm above the intercollicular groove of the medial malleolus. First, we drew a line tangential to the anterior border of the talus. We then drew reference line D perpendicular to this line. The angle between reference line D and the line tangential to the talar side of the medial malleolus was talar rotation (Fig. 6).

Measurement 20*: talar tilt.* To measure talar tilt, we set the coronal plane perpendicular to the bimalleolar axis. We chose the plane located at the center of the line connecting the most anterior and posterior aspects of the tibial plafond in the sagittal plane. The angle between 2 lines tangential to the tibial plafond and talar dome was talar tilt [35] (Fig. 7A). Negative values indicated talus inversion, and positive values indicated talar eversion.

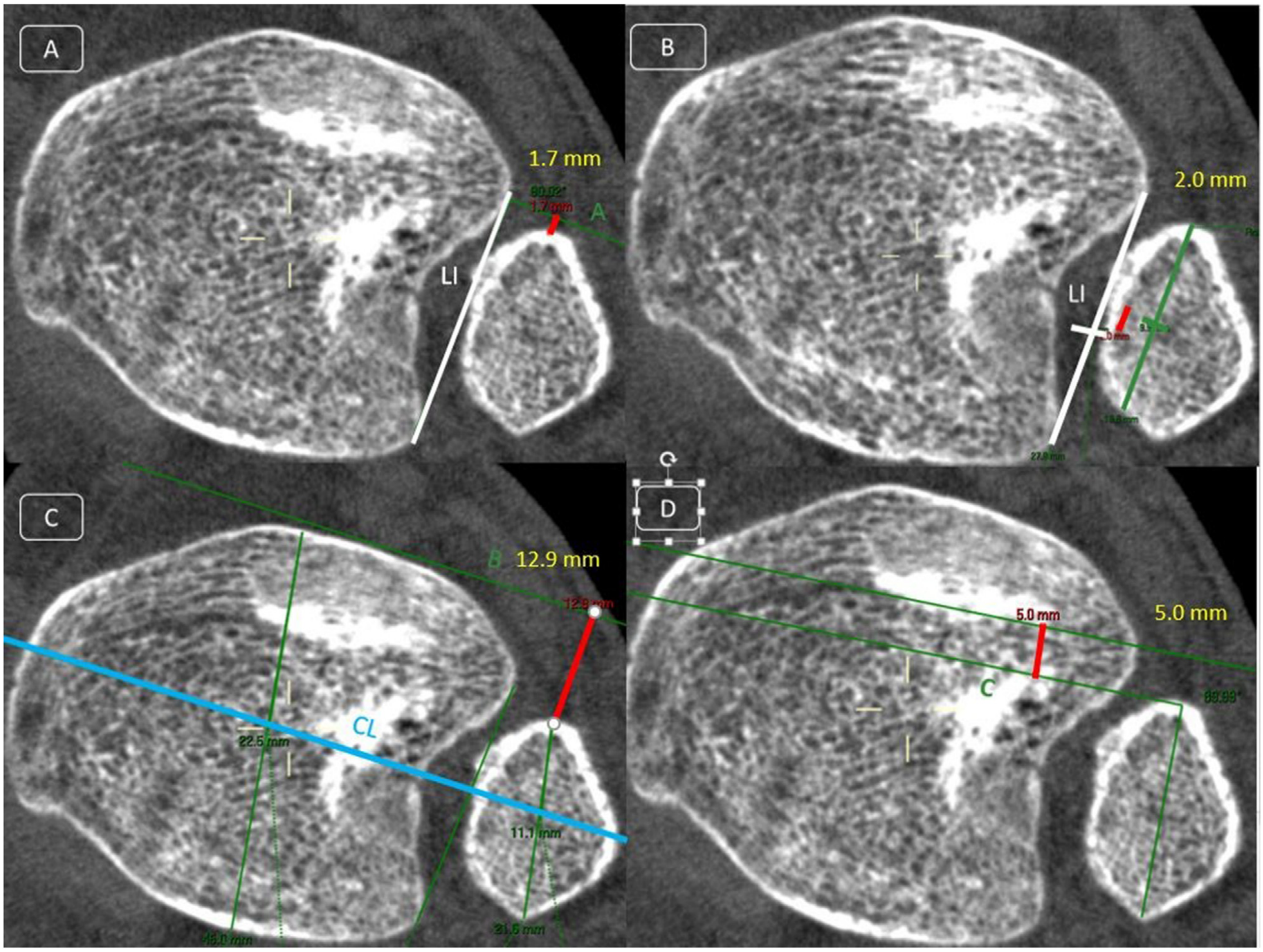

Fig. 4. Depiction of translation measurement. Axial images were set at 10 mm above the tibial plafond. (A) Fibular translation 1 (LI: tibial incisura length line). (B) Fibular translation 2. (C) Fibular translation 3 (CL: central line). (D) Fibular translation 4.

Measurement 21: fibular length. We performed the last measurement as described by Prior et al. [13]. We set the coronal plane perpendicular to the bimalleolar axis and selected the slice where fibular length was at its maximum. We then drew the anatomical axis of the fibula bisecting the fibular width. At the level of the most lateral part of the tibial plafond, we established reference line E as a line perpendicular to the fibular axis. The fibular length was determined by measuring the most distal aspect of the fibula to reference line E (Fig. 7B).

2.8. Statistical analysis

On the basis of the tibio-fibular distance determined from prior studies, we performed a power analysis [12,37]. Using a mean difference of 2.45 mm between the normal and injured ankles, 7 ankle pairs were required to detect a statistically significant difference with 80% power and an alpha level of 0.05. Values from each type of measurement were evaluated for normality of the data distribution by using the Shapiro–Wilk test. The intra-observer and inter-observer reliabilities of each measurement were obtained using intra-class correlation coefficients (ICCs), and the extent to which bias could reduce the ICC was considered. Correlations of 0.81–1.00 were considered perfect; 0.61–0.80 were substantial; 0.41–0.6 were moderate; 0.21–0.40 were fair; and $\leq$0.2 were poor [38,39]. To assess correlation between measurements obtained from WB and NWB images, we used Pearson or Spearman correlation, depending on the normality of data distribution. Measurements obtained from WB and NWB images were compared using paired Student t-tests or Wilcoxon rank-sum tests, depending on the normality of data. Because our sample size was relatively small, we applied bootstrapping or Monte Carlo simulation with 10,000 samples to obtain robust estimates of confidence intervals and P values for 99% uncertainty levels. P values were adjusted for multiple testing by using Benjamini-Hochberg corrections. Analysis was performed using PASW (version 20, Chicago, IL, USA) and Excel software (Microsoft Corp., Redmond, WA).

3. Results

3.1. Intra-observer and inter-observer reliability

3.1.1. Diastasis measurements

The intra-observer and inter-observer reliability of diastasis measurements are shown in Table 1. All measurements showed significant intra-observer and inter-observer reliability in both WB and NWB images ($P < 0.05$). Substantial to perfect agreement in both WB and NWB images was seen between observers 1 and 2, as well as between observers 2 and 3. Regarding the agreement between observers 1 and 3, all measurements showed substantial to perfect agreement except PTFD in WB images, which showed moderate agreement.

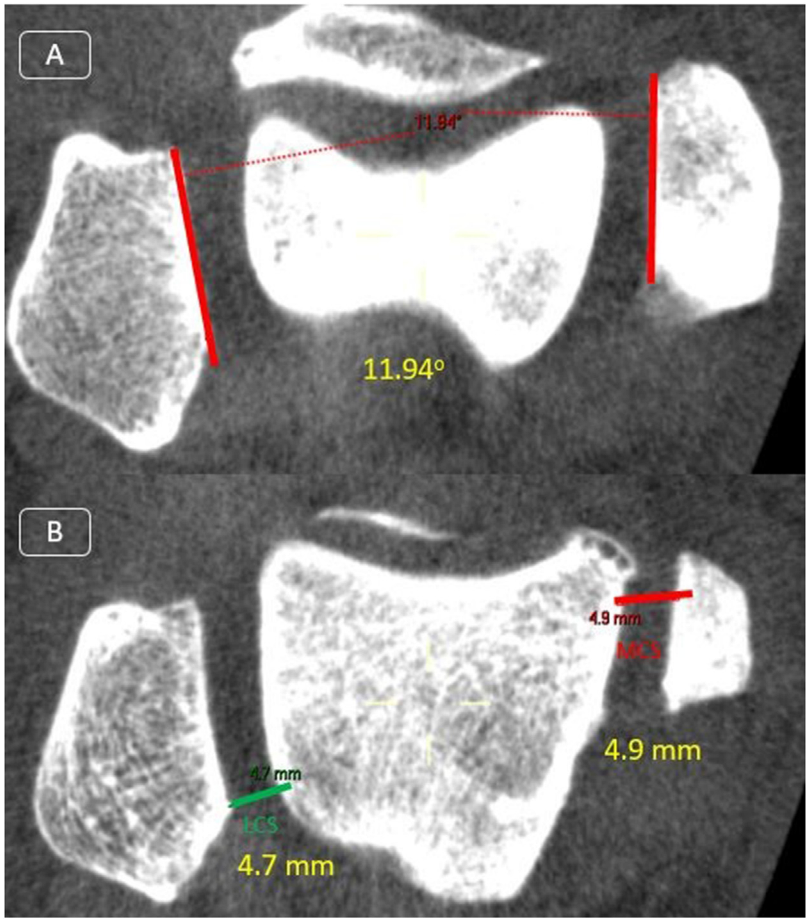

Fig. 5. Depiction of malleolar measurements. (A) Bimalleolar angle (B) MCS: medial clear space, LCS: lateral clear space.

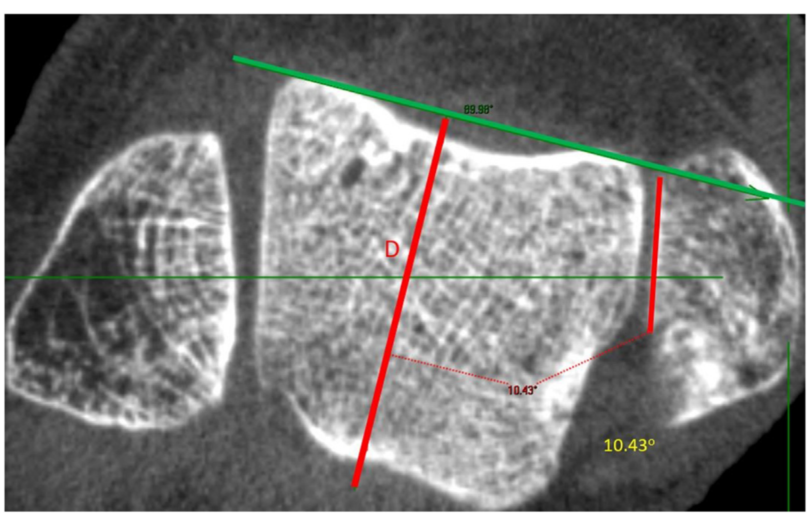

Fig. 6. Depiction of talar rotation measurement.

3.1.2. Rotation of the fibula

The intra-observer and inter-observer reliability of rotation measurements are shown in Table 2. All measurements showed significant intra-observer reliability in both WB and NWB images ($P < 0.05$). For observers 1 and 2, ICC values showed significant agreement, with substantial to perfect agreement for all measurements (except rotation of the fibula 3, with ICCs of 0.55 and 0.52 for WB and NWB images, respectively). For observers 1 and 3, ICC values showed significant agreement for all measurements except rotation

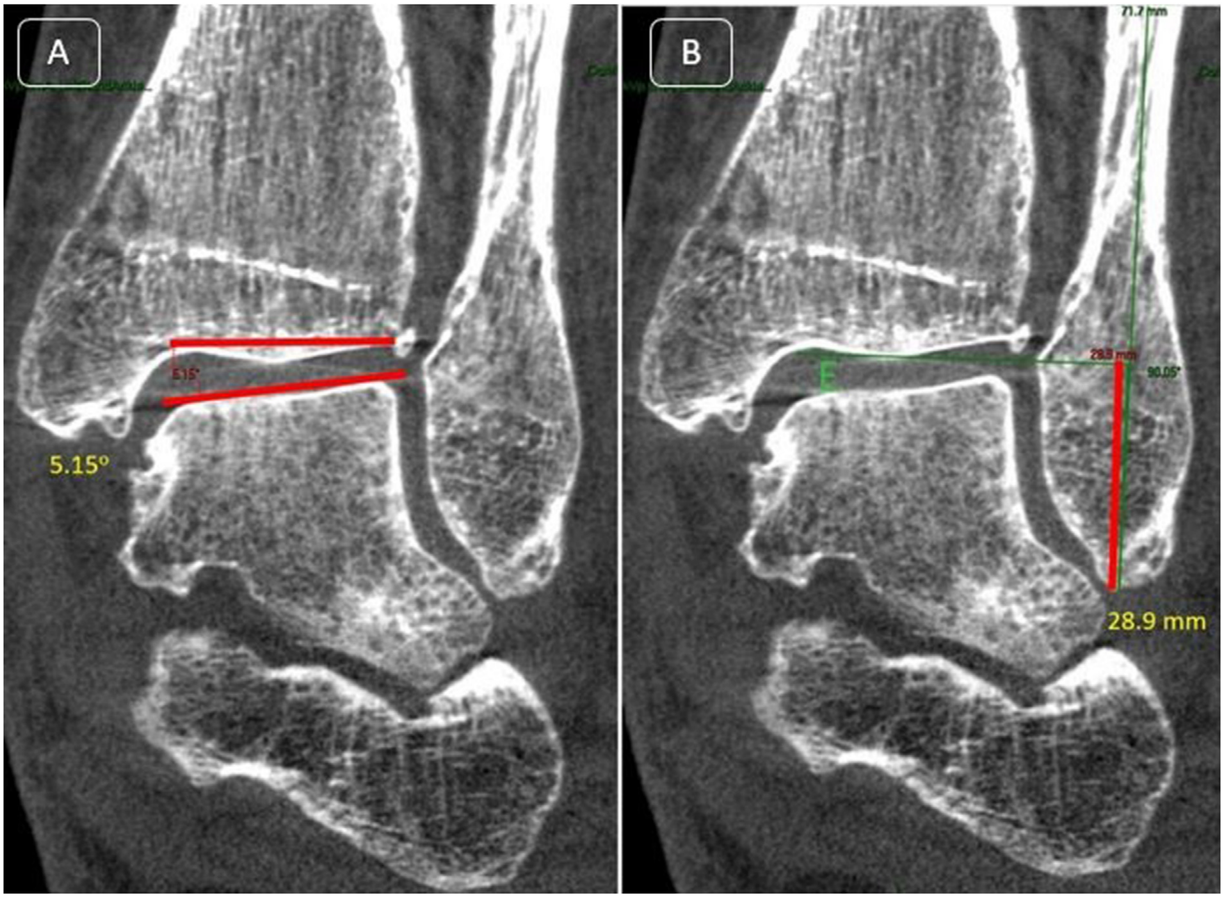

Fig. 7. (A) Depiction of talar tilt measurement. (B) Depiction of fibular length measurement.

Table 1
Intra-observer and inter-observer reliability of CT-based measurements of syndesmotic injury in 14 patients.

Measurements	Intra-observer reliability		Inter-observer reliability					
	WB	NWB	WB			NWB		
	ICC	ICC	ICC (R1–R2)	ICC 2 (R1–R3)	ICC 3 (R2–R3)	ICC (R1–R2)	ICC 2 (R1–R3)	ICC 3 (R2–R3)
ATFD[a]	0.97	0.94	0.87	0.82	0.84	0.90	0.66	0.73
PTFD	0.96	0.79	0.70	0.58	0.77	0.89	0.70	0.79
AW[a]	0.97	0.97	0.87	0.82	0.88	0.90	0.67	0.79
PW	0.93	0.93	0.91	0.74	0.84	0.85	0.73	0.84
TFCS	0.94	0.96	0.87	0.88	0.91	0.92	0.92	0.95
Diastasis	0.91	0.95	0.96	0.94	0.91	0.97	0.96	0.97
Angular measurement	0.86	0.94	0.90	0.93	0.88	0.84	0.94	0.88

ATFD: Anterior tibiofibular distance; AW: Anterior width; ICC: intra-class correlation; LCS: Lateral clear space; MCS: Medial clear space; NWB, non weight bearing; PTFD: Posterior tibiofibular distance; PW: Posterior width; TFCS: Tibiofibular clear space; WB: weight bearing.
Observer 1: MSK fellowship training radiologist 2. Foot and ankle fellowship training orthopaedic surgeon with 5 years of clinical experience 3. Foot and ankle fellowship training orthopaedic surgeon with 10 years of clinical experience.
ICC = 1.00 – 0.81 Perfect.
ICC = 0.80 – 0.61 Substantial.
ICC = 0.60 – 0.41Moderate.
ICC = 0.40 – 0.21 Fair.
ICC = 0.20 – 0.00 Poor.
[a] These measurements did not have normal distribution.

of fibula 3 in NWB images (ICC = 0.16; $P > 0.05$). There was significant agreement between observers 2 and 3 for all measurements except rotation of fibula 3 in NWB images (ICC = 0.21; $P > 0.05$).

3.1.3. Translation of the fibula

The intra-observer and inter-observer reliability of translation measurements are shown in Table 3. All measurements showed significant intra-observer reliability in both WB and NWB images ($P < 0.05$). Regarding inter-observer reliability, all ICC values were statistically significant. For observers 1 and 2, ICC values indicated moderate to perfect agreement for all WB and NWB measurements. For observers 1 and 3, ICC values indicated moderate to perfect agreement for all WB and NWB measurements. For observers 2 and 3, ICC values indicated moderate to perfect agreement for all WB and NWB measurements.

Table 2
Intra-observer and inter-observer reliability of CT-based measurements of syndesmotic injury in 14 patients.

Rotation of fibula	Intra-observer reliability		Inter-observer reliability					
	WB	NWB	Weight bearing			Non weight bearing		
	ICC	ICC	ICC (R1–R2)	ICC 2 (R1–R3)	ICC 3 (R2–R3)	ICC (R1–R2)	ICC 2 (R1–R3)	ICC 3 (R2–R3)
1	0.72	0.90	0.93	0.86	0.80	0.86	0.65	0.63
2	0.99	0.98	0.88	0.80	0.89	0.85	0.77	0.86
3	0.84	0.81	0.55	0.38	0.43	0.52	0.16[*]	0.21[*]
4	0.97	0.91	0.64	0.57	0.87	0.65	0.54	0.84

ICC: intra-class correlation; NWB, non weight bearing; WB: weight bearing.
Observer 1: MSK fellowship training radiologist 2. Foot and ankle fellowship training orthopaedic surgeon with 5 years of clinical experience 3. Foot and ankle fellowship training orthopaedic surgeon with 10 years of clinical experience.
ICC = 1.00–0.81 Perfect.
ICC = 0.80–0.61 Substantial.
ICC = 0.60–0.41 Moderate.
ICC = 0.40–0.21 Fair.
ICC = 0.20–0.00 Poor.
[*] P-value > 0.05.

Table 3
Intra-observer and inter-observer reliability of CT-based measurements of syndesmotic injury in 14 patients.

Fibular translation	Intra-observer reliability		Inter-observer reliability					
	WB	NWB	WB			NWB		
	ICC	ICC	ICC (R1–R2)	ICC 2 (R1–R3)	ICC 3 (R2–R3)	ICC (R1–R2)	ICC 2 (R1–R3)	ICC 3 (R2–R3)
1	0.96	0.96	0.91	0.87	0.92	0.82	0.64	0.84
2	0.96	0.98	0.72	0.63	0.53	0.45	0.45	0.63
3	0.89	0.91	0.72	0.57	0.70	0.57	0.77	0.78
4	0.98	0.97	0.65	0.61	0.91	0.79	0.70	0.72

ICC: intra-class correlation; NWB, non weight bearing; WB: weight bearing.
Observer 1: MSK fellowship training radiologist 2. Foot and ankle fellowship training orthopaedic surgeon with 5 years of clinical experience 3. Foot and ankle fellowship training orthopaedic surgeon with 10 years of clinical experience.
ICC = 1.00–0.81 Perfect.
ICC = 0.80–0.61 Substantial.
ICC = 0.60–0.41 Moderate.
ICC = 0.40–0.21 Fair.
ICC = 0.20–0.00 Poor.

Table 4
Intra-observer and inter-observer reliability of CT-based measurements of syndesmotic injury in 14 patients.

Measurements	Intra-observer reliability		Inter-observer reliability					
	WB	NWB	WB			NWB		
	ICC	ICC	ICC (R1–R2)	ICC 2 (R1–R3)	ICC 3 (R2–R3)	ICC (R1–R2)	ICC 2 (R1–R3)	ICC 3 (R2–R3)
Bimaleollar angle	0.95	0.69	0.67	0.49	0.61	0.67	0.60	0.80
MCS[a]	0.4	0.76	0.70	0.78	0.85	0.69	0.83	0.78
LCS[a]	0.96	0.95	0.58	0.73	0.70	0.66	0.85	0.73
Talar rotation[a]	0.95	0.97	0.78	0.31[*]	0.53	0.77	0.63	0.84
Talar tilt[a]	0.96	0.91	0.64	0.58	0.71	0.70	0.69	0.75
Fibular length	0.87	0.95	0.45	0.59	0.75	0.69	0.58	0.77

ICC: intra-class correlation; LCS: Lateral clear space; MCS: Medial clear space; NWB: non weight bearing; WB: weight bearing.
Observer 1: MSK fellowship training radiologist 2. Foot and ankle fellowship training orthopaedic surgeon with 5 years of clinical experience 3. Foot and ankle fellowship training orthopaedic surgeon with 10 years of clinical experience.
ICC = 1.00–0.81 Perfect.
ICC = 0.80–0.61 Substantial.
ICC = 0.60–0.41 Moderate.
ICC = 0.40–0.21 Fair.
ICC = 0.20–0.00 Poor.
[a] These measurements did not have normal distribution.
[*] P-value > 0.05

3.1.4. Other measurements

The intra-observer and inter-observer reliability of malleolar and talar measurements are shown in Table 4. All measurements showed significant intra-observer reliability in both WB and NWB images ($P < 0.05$). For observers 1 and 2, perfect to substantial agreement was noted for all measurements except LCS in WB images, which showed moderate agreement (ICC = 0.58). For observers 1 and 3, all measurements except talar rotation in WB images (ICC = 0.31, $P > 0.05$) showed significant agreement. For observers 2 and 3, perfect to substantial agreement was noted for all measurements except talar rotation in WB images, which showed moderate agreement (ICC = 0.53).

3.2. Comparison between WB and NWB measurements

Diastasis measurements obtained from WB and NWB images showed significant correlation (correlation coefficients (r) for ATFD, PTFD, AW, PW, TFCS, diastasis, and angular measurement were 0.71, 0.94, 0.64, 0.82, 0.96, 0.95, and 0.97, respectively). Rotation measurements obtained from WB and NWB images showed significant correlation (r for rotation of fibula 1, 2, 3, and 4 = 0.92, 0.83, 0.77, and 0.94, respectively). Except for fibular translation 2 (r = 0.28; P = 0.3), the remaining fibular translation measurements showed significant correlation between WB and NWB images (r for rotation of fibular translation 1, 3, and 4 = 0.56, 0.76, and 0.71, respectively). Talar rotation (r = 0.43; P = 0.1), talar tilt (r = 0.5; P = 0.06), and bimalleolar angle (r = 0.48; P = 0.08) measurements obtained from WB and NWB images were not significantly correlated. MCS (r = 0.7), LCS (r = 0.78), and fibular length (r = 0.94) measurements obtained from WB and NWB images were significantly correlated.

Mean WB and NWB measurements with their corresponding 95% confidence intervals (CIs) are shown in Table 5. Regarding diastasis measurements, we observed that mean PTFD (mean difference: 0.57 (95% CI: 0.29, 0.83); P = 0.04) and diastasis (mean difference: 0.39 (95% CI: 0.14, 0.69); P = 0.04) were significantly higher during WB. Mean angular measurement in WB images was significantly lower than in NWB images (mean difference: −2.66 (95%CI: −4.3, −0.9); P = 0.04). The remaining diastasis measurements did not change significantly when WB was applied.

Regarding rotation and translation measurements, no significant difference was observed between WB and NWB measurements (P > 0.05). Mean bimalleolar angle decreased significantly when WB was applied (mean difference: −4.32 (95% CI: −6.8, −1.9); P = 0.04). There were no significant differences between mean MCS, LCS, talar rotation, or talar tilt between WB and NWB measurements (P > 0.05). Mean fibular length in WB images was significantly lower than NWB images (mean difference: −0.94 (95% CI: −1.4, 4 – 0.46) P = 0.04).

4. Discussion

The findings of this study demonstrate that, under WB, syndesmotic measurements are feasible and reproducible and have a high level of agreement between different observers. The current report describes one of the few assessments of distal tibiofibular syndesmosis under physiologic WB. Our study is the first attempt to evaluate the reliability and reproducibility of 21 syndesmosis measurements using WB CBCT images and to compare them with NWB measurements.

Cadaver studies have shown that the fibula plays an important role in weightbearing by carrying approximately 6.4%–30% of the axial load, and it has been suggested that fibular loading varies under abnormal conditions, such as syndesmotic injury [40–42]. Despite the major effect of loading on the biomechanics of the tibio-talar joint, as well as the distal tibio-fibular syndesmosis, few studies have evaluated the effect of load on live human patients by using advanced imaging modalities such as CT, and there are no data regarding the reliability of syndesmosis measurements using WB CT [17,43].

The high level of intra- and inter-observer reliability observed in our study could be attributable to the fact that our observers

Table 5
Mean and confidence intervals of syndesmosis measurements and their comparison between weight bearing and non-weight bearing images.

Measurements	WB images mean/ median	95% CI/ IQR	NWB images mean/ median	95% CI/ IQR	Mean of difference (95% CI/range of difference[a])	P-value after bootstrapping	(BH) corrections
ATFD[a]	4.25	2.39	4.02	1.93	0.73 (0.15, 1.3)	0.04	0.1
PTFD	4.89	3.9, 5.8	4.3	3.4, 5.1	**0.57** (**0.29, 0.83**)	**0.003**	**0.04**
AW[a]	3.95	1.8	3.65	1.54	0.64 (0.06, 1.2)	0.05	0.1
PW	6.03	5.0–7.0	5.97	4.9–7	0.06 (−0.46, 0.6)	0.8	0.9
TFCS	4.12	3.14–5.1	3.81	2.9–4.7	0.30 (0.13, 0.52)	0.02	0.06
Diastasis	4.01	2.9–5.0	3.61	2.6–4.6	**0.39** (**0.14, 0.69**)	**0.01**	**0.04**
Angular measurement	61.63	54.6–68.64	64.29	56.4–72.1	**−2.66** (**−4.3, −0.9**)	**0.01**	**0.04**
Rotation of fibula							
1	49.50	42.9, 56.0	50.43	44.7, 56.1	0.08 (−1.9, 2.1)	0.4	0.6
2	4.69	−4.3, 13.7	8.29	−0.16, 16.7	−2.5 (−6, 1.08)	0.2	0.3
3	7.66	1.09, 14.2	7.89	3.3, 12.4	0.87 (−2.4, 4.2)	0.9	0.9
4	0.92	0.87–0.97	0.93	0.88–0.98	−0.009 (−0.02, 0.003)	0.1	0.2
Fibular translation							
1	1.76	0.59–2.94	1.79	1.0–2.5	−0.02 (−0.93, 0.76)	0.9	0.9
2	0.68	1.72	1.4	2.1	−0.2 (−1, 0.65)	0.5	0.6
3	9.71	8.9–10.5	9.94	9.2–10.6	−0.22 (−0.7, 0.22)	0.3	0.5
4	2.51	1.6–3.3	2.70	1.9–3.4	−0.19 (−0.7, 0.29)	0.4	0.6
Bimaleollar angle	7.67	5–10.3	11.9	9.1–14.8	**−4.32** (**−6.8, −1.9**)	**0.006**	**0.04**
MCS[a]	2.48	0.72	2.61	0.63	0.15(−0.1, 0.46)	0.7	0.8
LCS[a]	2.75	1.38	2.9	1.73	−0.25 (−0.5, −0.03)	0.02	0.06
Talar rotation	5.84	1.9, 9.7	6.01	3.6,8.3	−0.16 (−3.0, 2.9)	0.9	0.9
Talar tilt[a]	−0.56	1.98	−0.03	2.3	−0.27 (−0.91, 0.4)	0.5	0.6
Fibular length	23.39	21.8–24.8	24.33	22.5–26	**−0.94** (**−1.4, −0.46**)	**0.005**	**0.04**

ATFD: Anterior tibiofibular distance; AW: Anterior width; CI: confidence interval; IQR: interquartile range; IQR: Inter-quartile range; LCS: Lateral clear space; MCS: Medial clear space; PTFD: Posterior tibiofibular distance; PW: Posterior width; TFCS: Tibiofibular clear space.
The bold values represent statstically significant difference between weightbearing and non-weightbearing images.
[a] These measurements did not have normal distribution.

underwent training that familiarized them with anatomical landmarks, measurement techniques, and the measurement software. Furthermore, we used the novel technique of multi-planar reconstruction (MPR) to determine the level at which measurements were obtained. In this way, we confirmed that these measurements were obtained at the exact level of a predetermined plane, and factors such as ankle rotation and reader's bias did not affect our measurements. Thus, it can be assumed that the predefined anatomical landmarks were consistent across all examinations. This is particularly important in a region such as the incisura fibularis, which has known to be highly variable, and it is reflected in our findings, which showed that TFCS, diastasis, and angular measurement were associated with perfect intra- and inter-observer reliability.

Regarding rotation measurements, fibular rotation 1 and 2 showed substantial to perfect agreement. This finding agrees with those of previous studies [9,17,44]. In contrast, fibular rotation 4 involved determining the center point of the tibial surface by using multiple lines, and this could have led to the lower level of agreement we found (ICC range: 0.54, 0.87). Fibular rotation 3 also involved drawing a tangential line over the anterior tibial surface, which our observers found challenging, which could have caused the poor agreement between observers.

Although studies have reported a high level of agreement for different fibular translation measurements [13,14,17,34], we observed that only fibular translation 1 had substantial to perfect agreement. We attribute this finding to the simplicity of our method. Other translation measurements involved drawing multiple lines, which could have increased the level of random error. The same concept applies to talar rotation, because finding the predefined plane in ankles with prior injuries was difficult for observers.

Other measurements, such as talar tilt, bimalleolar angle, LCS, and MCS showed moderate to perfect reliability between observers. This was likely because these measurements were described vaguely, and certain anatomical landmarks were not determined. Further studies are needed to identify well-designed, reliable measurements addressing the same concept.

Fibular length measurement was associated with fair to substantial reliability in our study (ICC range: 0.45, 0.75). The importance of fibular length should be emphasized by the effect of axial loading has on the biomechanics of ankle joint. The fibula has been found to be a major contributor to ankle mortise stability. The syndesmosis ligaments stabilize the fibula to the tibia and assist in maintaining the integrity of the ankle joint, as well [42,45]. During WB, an average of 2.4 mm of fibular downward migration has been reported, which deepens the ankle mortise, tightens syndesmosis ligaments, and pulls the fibula medially. These alterations during WB give further lateral support to the ankle joint during gait, particularly throughout stance and push-off phases. Therefore, it could be assumed that, after syndesmotic injury, the fibula is no longer stabilized, ankle stability is lost, and the fibula moves upward and laterally during WB. However, the description of fibular length measurement was poor, and no defined plane was described to evaluate this critical measurement. Our observers had difficulty finding the optimal plane for these measurements, and we assume this could have led to low reliability.

Our study has several important limitations. First, we were unable to scan the contralateral ankles of our patients. Therefore, it is unknown whether these measurements in normal ankles vary between WB and NWB images. However, a previous study evaluating the normal syndesmosis confirmed that, with WB, the intact syndesmosis prevents widening of distal tibio-fibular joint as measured by AW, PW, TFCS, fibular translation 2, and rotation of fibula 1. Second, our patients did not undergo arthroscopy to confirm syndesmotic injuries. Thus, our measurements could reflect average values based on stable and unstable syndesmoses. The purpose of this study was not to determine the diagnostic accuracy of these measurements; rather, it was to assess the feasibility and reliability of syndesmosis measurements in patients with prior ankle injuries using WB CBCT. We did not intend to compare the normal versus abnormal ranges of these measurements. Third, our patients had a heterogeneous collection of ankle fractures based on Weber classification. Because the value of prior ankle fracture classification systems in predicting the instability of fractures and in choosing treatments has been shown to be limited, we excluded fractures that were unstable and underwent operative treatment and included fractures that were stable at the first clinic visit to make our study population more homogenous. We did not intend to report syndesmosis measurements in distinct types of ankle injuries or fractures. Finally, because we had neither normal contralateral ankle measurements nor information regarding the arthroscopic findings of our patients, we could not determine that the observed difference between our measurements in WB and NWB were attributable to an injured syndesmosis rather than a consequence of loading on the normal syndesmosis. We cannot determine the clinical importance and diagnostic accuracy of these measurements, which should be addressed by studies with arthroscopic findings and data from normal contralateral ankles.

5. Conclusion

In patients with prior ankle injuries, syndesmosis measurements using WB CT images are feasible, reproducible, and have a high level of agreement between observers. Our data suggest that TFCS, diastasis, angular measurement, translation of fibula 1, and rotation of fibula 1 and 2 had high intra- and inter-observer reliability. Among these measurements, PTFD, diastasis, and angular measurement were significantly different between WB and NWB images. Clinical studies examining these measurements under WB and NWB conditions, in patients with confirmed syndesmosis injury and available data on normal contralateral ankles, are required to determine whether this difference was caused by physiologic loading or syndesmotic instability.

Conflict of interest

- Greg M Osgood: Research support from Carestream Health
- Delaram Shakoor: Nothing to disclose
- Jakrapong Orapin: Nothing to disclose
- Jianzhong Qin: Nothing to disclose
- Iman Khodarahmi: Nothing to disclose
- Gaurav K Thawait: Nothing to disclose
- James R Ficke: Nothing to disclose
- Lew C schon: Research support from Zimmer/Biomet, Carestream Health, Wright Medicalm, Smith-Nephew and pine-Smith/Celing Bioscience.
- Shadpour Demehri: Research support from General Electric Company and Carestream Health, Inc. Grants from GERRAF. Consultant to Toshiba Corporation

References

[1] Huber T., Schmoelz W, Bolderl A. Motion of the fibula relative to the tibia and its alterations with syndesmosis screws: a cadaver study. Foot Ankle Surg 2012;18:203.

[2] Hermans JJ, Beumer A, de Jong TA, Kleinrensink GJ. Anatomy of the distal tibiofibular syndesmosis in adults: a pictorial essay with a multimodality approach. J Anat 2010;217:633.

[3] Fort NM, Aiyer AA, Kaplan JR, Smyth NA, Kadakia AR. Management of acute injuries of the tibiofibular syndesmosis. Eur J Orthop Surg Traumatol 2017;27:449.

[4] Ebinger T, Goetz J, Dolan L, Phisitkul P. 3D model analysis of existing CT syndesmosis measurements. Iowa Orthop J 2013;33:40.
[5] Sagi HC, Shah AR, Sanders RW. The functional consequence of syndesmotic joint malreduction at a minimum 2-year follow-up. J Orthop Trauma 2012;26:439.
[6] Yeung TW, Chan CY, Chan WC, Yeung YN, Yuen MK. Can pre-operative axial CT imaging predict syndesmosis instability in patients sustaining ankle fractures? Seven years' experience in a tertiary trauma center. Skeletal Radiol 2015;44:823.
[7] Ebraheim NA, Lu J, Yang H, Mekhail AO, Yeasting RA. Radiographic and CT evaluation of tibiofibular syndesmotic diastasis: a cadaver study. Foot Ankle Int 1997;18:693.
[8] Gardner MJ, Demetrakopoulos D, Briggs SM, Helfet DL, Lorich DG. Malreduction of the tibiofibular syndesmosis in ankle fractures. Foot Ankle Int 2006;27:788.
[9] Dikos GD, Heisler J, Choplin RH, Weber TG. Normal tibiofibular relationships at the syndesmosis on axial CT imaging. J Orthop Trauma 2012;26:433.
[10] Nault ML, Hebert-Davies J, Laflamme GY, Leduc S. CT scan assessment of the syndesmosis: a new reproducible method. J Orthop Trauma 2013;27:638.
[11] Han SH, Lee JW, Kim S, Suh JS, Choi YR. Chronic tibiofibular syndesmosis injury: the diagnostic efficiency of magnetic resonance imaging and comparative analysis of operative treatment. Foot Ankle Int 2007;28:336.
[12] Elgafy H, Semaan HB, Blessinger B, Wassef A, Ebraheim NA. Computed tomography of normal distal tibiofibular syndesmosis. Skeletal Radiol 2010;39:559.
[13] Prior CP, Widnall JC, Rehman AK, Weller DM, Wood EV. A simplified, validated protocol for measuring fibular reduction on ankle CT. Foot Ankle Surg 2017;23:53.
[14] Davidovitch RI, Weil Y, Karia R, Forman J, Looze C, Liebergall M, Egol K. Intraoperative syndesmotic reduction: three-dimensional versus standard fluoroscopic imaging. J Bone Joint Surg Am 2013;95:1838.
[15] Sarsam IM, Hughes SP. The role of the anterior tibio-fibular ligament in talar rotation: an anatomical study. Injury 1988;19:62.
[16] Beumer A, Valstar ER, Garling EH, Niesing R, Ginai AZ, Ranstam J, et al. Effects of ligament sectioning on the kinematics of the distal tibiofibular syndesmosis: a radiostereometric study of 10 cadaveric specimens based on presumed trauma mechanisms with suggestions for treatment. Acta Orthop 2006;77:531.
[17] Lepojarvi S, Niinimaki J, Pakarinen H, Leskela HV. Rotational dynamics of the normal distal tibiofibular joint with weight-bearing computed tomography. Foot Ankle Int 2016;37:627.
[18] Kim JB, Yi Y, Kim JY, Cho JH, Kwon MS, Choi SH, et al. Weight-bearing computed tomography findings in varus ankle osteoarthritis: abnormal internal rotation of the talus in the axial plane. Skeletal Radiol 2017;46:1071.
[19] de Cesar Netto C, Schon LC, Thawait GK, da Fonseca LF, Chinanuvathana A, Zbijewski WB, et al. Flexible adult acquired flatfoot deformity: comparison between weight-bearing and non-weight-bearing measurements using cone-beam computed tomography. J Bone Joint Surg Am 2017;99:e98.
[20] Osgood GM, Thawait GK, Hafezi-Nejad N, Shakoor D, Shaner A, Yorkston J, et al. Image quality of cone beam computed tomography for evaluation of extremity fractures in the presence of metal hardware: visual grading characteristics analysis. Br J Radiol 2017;90: 20160539.
[21] Lintz F, de Cesar Netto C, Barg A, Burssens A, Richter M. Weight-bearing cone beam CT scans in the foot and ankle. EFORT Open Rev 2018;3:278.
[22] Richter M, Lintz F, Zech S, Meissner SA. Combination of PedCAT weightbearing CT with pedography assessment of the relationship between anatomy-based foot center and force/pressure-based center of gravity. Foot Ankle Int 2018;39:361.
[23] Richter M, Seidl B, Zech S, Hahn S. PedCAT for 3D-imaging in standing position allows for more accurate bone position (angle) measurement than radiographs or CT. Foot Ankle Surg 2014;20:201.
[24] Fox A, Wykes P, Eccles K, Barrie J. Five years of ankle fractures grouped by stability. Injury 2005;36:836.
[25] Pakarinen HJ, Flinkkil TE, Ohtonen PP, Ristiniemi JY. Stability criteria for nonoperative ankle fracture management. Foot Ankle Int 2011;32:141.
[26] Carrino JA, Al Muhit A, Zbijewski W, Thawait GK, Stayman JW, Packard N, et al. Dedicated cone-beam CT system for extremity imaging. Radiology 2013;270:816.
[27] American Association of Physicists in Medicine. Comprehensive methodology for the evaluation of radiation does in x-ray computed tomography. AAPM Report No. 111. Available at http://www.aapm.org/pubs/reports/RPT_111. pdf. [Accessed 28 July 2017].
[28] Lepojarvi S, Pakarinen H, Savola O, Haapea M, Sequeiros RB, Niinimaki J. Posterior translation of the fibula may indicate malreduction: CT study of normal variation in uninjured ankles. J Orthop Trauma 2014;28:205.
[29] Malhotra G, Cameron J, Toolan BC. Diagnosing chronic diastasis of the syndesmosis: a novel measurement using computed tomography. Foot Ankle Int 2014;35:483.
[30] Zwipp H. Chirurgie des Fusses. Wien: Springer-Verlag; 1994.
[31] Vasarhelyi A, Lubitz J, Gierer P, Gradl G, Rosler K, Hopfenmuller W, et al. Detection of fibular torsional deformities after surgery for ankle fractures with a novel CT method. Foot Ankle Int 2006;27:1115.
[32] Knops SP, Kohn MA, Hansen EN, Matityahu A, Marmor M. Rotational malreduction of the syndesmosis: reliability and accuracy of computed tomography measurement methods. Foot Ankle Int 2013;34:1403.
[33] Tang CW, Roidis N, Vaishnav S, Patel A, Thordarson DB. Position of the distal fibular fragment in pronation and supination ankle fractures: a CT evaluation. Foot Ankle Int 2003;24:561.
[34] Phisitkul P, Ebinger T, Goetz J, Vaseenon T, Marsh JL. Forceps reduction of the syndesmosis in rotational ankle fractures: a cadaveric study. J Bone Joint Surg Am 2012;94:2256.
[35] Lepojarvi S, Niinimaki J, Pakarinen H, Koskela L, Leskela HV. Rotational dynamics of the talus in a normal tibiotalar joint as shown by weight-bearing computed tomography. J Bone Joint Surg Am 2016;98:568.
[36] Pelton K, Thordarson DB, Barnwell J. Open versus closed treatment of the fibula in Maissoneuve injuries. Foot Ankle Int 2010;31:604.
[37] Mukhopadhyay S, Metcalfe A, Guha AR, Mohanty K, Hemmadi S, Lyons K, et al. Malreduction of syndesmosis–are we considering the anatomical variation? Injury 2011;42:1073.
[38] Ellis SJ, Deyer T, Williams BR, Yu JC, Lehto S, Maderazo A, et al. Assessment of lateral hindfoot pain in acquired flatfoot deformity using weightbearing multiplanar imaging. Foot Ankle Int 2010;31:361.
[39] Landis JR, Koch GG. The measurement of observer agreement for categorical data. Biometrics 1977;33:159.
[40] Takebe K, Nakagawa A, Minami H, Kanazawa H, Hirohata K. Role of the fibula in weight-bearing. Clin Orthop Related Res 1984;289.
[41] Wang Q, Whittle M, Cunningham J, Kenwright J. Fibula and its ligaments in load transmission and ankle joint stability. Clin Orthop Related Res 1996;261.
[42] Norkus SA, Floyd RT. The anatomy and mechanisms of syndesmotic ankle sprains. J Athl Train 2001;36:68.
[43] Marzo JM, Kluczynski MA, Clyde C, Anders MJ, Mutty CE, Ritter CA. Weight bearing cone beam CT scan versus gravity stress radiography for analysis of supination external rotation injuries of the ankle. Quant Imaging Med Surg 2017;7:678.
[44] Ahn TK, Choi SM, Kim JY, Lee WC. Isolated syndesmosis diastasis: computed tomography scan assessment with arthroscopic correlation. Arthroscopy 2017;33:828.
[45] Scranton Jr. PE, McMaster JG, Kelly E. Dynamic fibular function: a new concept. Clin Orthop Related Res 1976;76.